EFFECTS ON FLAT-BEAM GENERATION FROM SPACE-CHARGE FORCE AND BEAMLINE ERRORS

Y.-E Sun*, K.-J. Kim†, University of Chicago, Chicago, IL 60637, USA
P. Piot, Fermilab, Batavia, IL 60510, USA

Abstract

The transformation of a round, angular-momentum-dominated electron beam produced in a photoinjector into a flat beam using a transformer composed of three skew-quadrupoles [1] has been developed theoretically [2, 3] and experimentally [4]. In this paper, we present numerical and analytical studies of space-charge forces, and evaluate the corresponding limits on the ratio of vertical-to-horizontal emittances. We also investigate the sensitivities of flat-beam emittances on the quadrupole misalignments in each of the six degrees of freedom.

SPACE-CHARGE EFFECTS

We will first present the space-charge effects in flat-beam generation as seen in simulations. An analytical approach then follows, where we estimate the emittance growth caused by the nonlinear space-charge force and the resulting limitation on flat-beam production.

Simulations

Modeling the beamline of the Fermilab/NICADD[1] Photoinjector Laboratory (FNPL) (see Figure 1) with the parameters listed in Table 1, ASTRA [5] simulations were performed with the space-charge force on and off, and the quadrupole strengths are adjusted accordingly in each case.

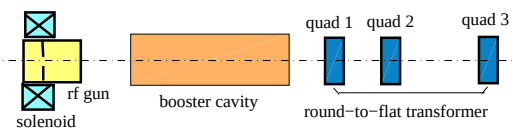

Figure 1: Schematic drawing of FNPL beamline.

An emittance ratio larger than 1200 is obtained with the space-charge off, compared to $\sim$ 300 with space-charge on; see Figure 2.

Apart from space-charge on/off from start to end, another interesting case is having the space-charge on only prior to the round-to-flat transformer, as shown with the dash-dot line in Figure 2. We see it is closer to the case where space charge is on all the way. It is thus reasonable to conclude that space-charge effects are more important prior to than during and/or after the transformer. This correlates to the space-charge force being proportional to $1/\gamma^2$, since during/after the transformer, the beam energy already reached its maximum in the beamline ($\sim$ 17 MeV). Space charge is especially important in the rf gun, where kinetic energy increases from almost zero at the photocathode to about 4 MeV at the gun exit.

Table 1: FNPL machine parameters used in simulation.

parameter	value	units
rms laser pulse (Gaussian) length	3	ps
thermal energy at cathode	0.75	eV
magnetic field on cathode B_0	$\sim$935	Gauss
rms beam size on cathode σ_c	0.80	mm
bunch charge Q	0.50	nC
gun rf phase	25	degree
gun peak gradient	35	MV/m
booster cavity peak gradient	25	MV/m

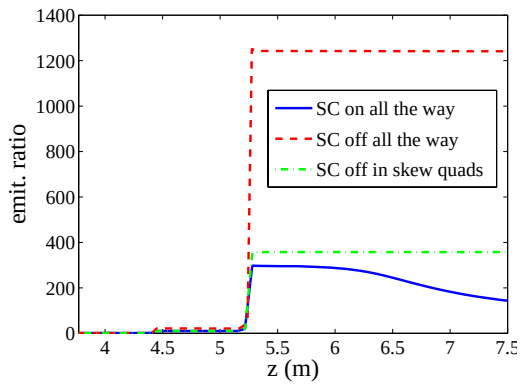

Figure 2: Effect of space charge on the emittance ratio.

Analytics

In this Section we will discuss space-charge induced emittance growth in the rf gun and its corresponding influence on flat-beam generation. Take, as a model, the space charge force to be

$$F_r \propto ar + br^3, \tag{1}$$

or in Cartesian coordinates,

$$\begin{aligned} F_x &\propto ax + bx(x^2 + y^2), \\ F_y &\propto ay + by(x^2 + y^2). \end{aligned} \tag{2}$$

* yinesun@uchicago.edu
† also ANL, Argonne, IL 60439, USA

[1] NICADD is an acronym for Northern Illinois Center for Accelerator and Detector Development.

The change to the dimensionless momentum $p_x = \gamma v_x/c$ caused by F_x is

$$\Delta p_x = \frac{1}{mc}\int F_x \mathrm{d}t \approx \frac{1}{mc^2}\int \frac{F_x}{\beta}\mathrm{d}z, \qquad (3)$$

where m is electron rest mass, c is the speed of light in vacuum, $\beta = v/c$ and γ is the Lorentz factor. Since the space-charge force is most significant during a short interval from the cathode surface, we can assume that the electron's transverse coordinates remain constant in the rf gun, and Δp_x and Δp_y can be written as

$$\Delta p_x = ax + bx^3 + bxy^2, \quad \Delta p_y = ay + by^3 + bx^2 y. \quad (4)$$

The initial phase-space coordinates of the angular-momentum-dominated beam are given by [3]

$$X = \begin{bmatrix} x \\ p_x - \kappa y \end{bmatrix}, \quad Y = \begin{bmatrix} y \\ p_y + \kappa x \end{bmatrix}, \qquad (5)$$

where $\kappa = B_0/(2mc)$, B_0 is the axial magnetic field on the cathode. Adding Eq. (4) to the second rows of Eq. (5) respectively, and assuming that $\langle xp_x\rangle = \langle xp_y\rangle = \cdots = 0$ ("$\langle\ \rangle$" meaning to take the average over the beam distribution), the beam matrix is

$$\Sigma_{n,sc} = \begin{bmatrix} \varepsilon_{sc}T_{sc} & \mathcal{L}J \\ -\mathcal{L}J & \varepsilon_{sc}T_{sc} \end{bmatrix}, \qquad (6)$$

where

$$\varepsilon_{sc}^2 = \varepsilon^2 + b^2\Lambda, \quad \Lambda = \sigma^2\sigma_6 + \sigma^4\sigma_4 - \sigma^8 - \sigma_4^2. \quad (7)$$

Here $\sigma^2 = \langle x^2\rangle = \langle y^2\rangle$, $\mathcal{L} = \kappa\sigma^2$, $\varepsilon = \sigma\sqrt{{p_x}^2 + (\kappa\sigma)^2}$, $\sigma_n = \langle x^n\rangle$, T_{sc} is a 2×2 matrix whose determinant is one, and J is the 2×2 unit symplectic matrix given by:

$$J = \begin{bmatrix} 0 & 1 \\ -1 & 0 \end{bmatrix}. \qquad (8)$$

Immediately we see from Eq. (6) that the uncorrelated emittance increases due to the nonlinear space-charge force through parameter b; however the parameter $\mathcal{L}$ which is related to the beam angular momentum remains unaffected. This can be understood since the space-charge force, linear or not, is in the radial direction, hence preserves the cylindrical symmetry and thus conserves the angular momentum.

The normalized flat-beam emittances change correspondingly from $\varepsilon^{\pm}$ to $\varepsilon_{sc}^{\pm}$:

$$\varepsilon^{\pm} = \sqrt{\varepsilon^2 + \mathcal{L}^2} \pm \mathcal{L} \Rightarrow \varepsilon_{sc}^{\pm} = \sqrt{\varepsilon_{sc}^2 + \mathcal{L}^2} \pm \mathcal{L}. \quad (9)$$

Next, we work out the case for a long beam whose transverse profile is Gaussian. Write the charge density as:

$$\rho(r) = \rho_0 e^{-\frac{r^2}{2\sigma_r^2}} \approx \rho_0(1 - \frac{r^2}{2\sigma_r^2} + \cdots), \qquad (10)$$

where $\rho_0 = Q/(2\pi\sigma_r^2 l_z)$ is the normalization factor, with Q and l_z being the bunch charge and length. Only the first two terms of the expansion are considered in the following discussion. In reality, the transverse profile is taken to be a truncated Gaussian, and we can write the charge density

$$\rho(r) = \rho_0(1 - b^*\frac{r^2}{2\sigma_r^2}), \qquad (11)$$

where the factor b^* can be determined from the beam distribution. In Figure 3, the dots pertain to the observed $\rho(r)$ for a typical beam used in flat-beam experiments, and the solid line is a fit in the form of Eq. (11); b^* is found to be 0.3 in this case.

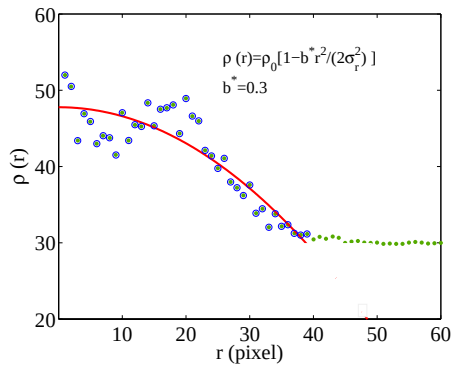

Figure 3: A typical beam density profile along radial direction as observed experimentally (dots) at the photocathode. The solid line is a fit in the form of Eq. (11) for the circled dots.

From Gauss's law, we have the radial electric field given by

$$E_r = \frac{\rho_0 r}{2\epsilon_0}(1 - b^*\frac{r^2}{4\sigma_r^2}) \qquad (12)$$

From Amperes law, we have the magnetic field $B_\theta = (\mu_0 v r\rho)/(2) = E_r\beta/c$. The Lorentz force is then given by:

$$F_r = \frac{eE_r}{\gamma^2}. \qquad (13)$$

Upon substituting Eqs. (12) and (13) into Eq. (4), we have:

$$\Delta p_x = \frac{I}{I_0}\frac{\mathcal{I}}{\sigma_r^2}x(1 - b^*\frac{x^2+y^2}{4\sigma_r^2}), \qquad (14)$$

where $\mathcal{I} = \int \mathrm{d}z/(\beta\gamma^2)$ and I_0 is the Alfvén current for electrons. To calculate the integral $\mathcal{I}$ [6], let's assume the energy gain is linear, i.e., $d\gamma/dz = (\gamma_f - 1)/z_f$ where γ_f and z_f the Lorentz factor and z coordinate at the gun exit; we have

$$\mathcal{I} = \frac{z_f}{\gamma_f - 1}\int \frac{1}{\beta\gamma^2}\mathrm{d}\gamma = \frac{z_f}{\gamma_f - 1}(\frac{\pi}{2} - \sin^{-1}\frac{1}{\gamma_f}). \quad (15)$$

In the case of a $(n + \frac{1}{2})$-cell rf gun, we have $z_f = (n + \frac{1}{2})\lambda/2$, where λ is the rf wavelength.

Eq. (14) is of the form Eq. (4) with the following identifications:

$$a = \frac{I}{I_0}\frac{\mathcal{I}}{2\sigma^2}, \quad b = -b^*\frac{I}{I_0}\frac{\mathcal{I}}{16\sigma^4}, \qquad (16)$$

where we used $\sigma_r^2 = 2\sigma^2$ for a cylindrically symmetric beam.

From the distribution given by Eq. (10), we obtain

$$\Lambda = 8\sigma^8. \tag{17}$$

Finally, substituting Eq. (16) and Eq. (17) into Eq. (9), we get

$$\varepsilon_{sc} = \sqrt{\left(b^* \frac{I}{I_0} \frac{\mathcal{I}}{4\sqrt{2}}\right)^2 + \varepsilon^2}. \tag{18}$$

Take the following typical parameters at FNPL: $b^* = 0.3$, $I = 35$ A, $\gamma_f = 9$, $z_f \approx 0.17$ m for a 1.5-cell 1.3 GHz rf gun, normalized thermal emittance $\varepsilon = 1$ μm. From Eq. (18), we obtain $\varepsilon_{sc} = 3.53$ μm. If $\mathcal{L} = 20$ μm, due to the nonlinear space-charge force, the smaller of the two transverse flat-beam emittances increases from 0.02 to 0.30 μm, and the corresponding emittance ratio drops from 2000 to 130.

In reality, particle transverse positions change under the space-charge and external electromagnetic forces, and the energy gain is not linear along z-axis, so that the beam dynamics is much more complicated. Nevertheless the discussion here shows that the emittance growth caused by nonlinear space charge in the rf gun is the major limiting factor on achieving a flat beam with very small emittance and high emittance ratio.

BEAMLINE ERRORS

We numerically studied the effects on flat beam ratio caused by the quadrupole alignment error. This includes the rotational errors around x, y and z axes, and the displacements $\mathrm{d}x$, $\mathrm{d}y$ and $\mathrm{d}z$ of each quadrupole; see Figure 1.

The rotation angle around the longitudinal axis should be 45° for a skew quadrupole. In Figure 4 (a), we scan the tilt angle of each quadrupole by $\pm 2^\circ$ in simulation. The emittance ratio is more sensitive to the first and second quadrupole tilt angles, and much less sensitive to the third one.

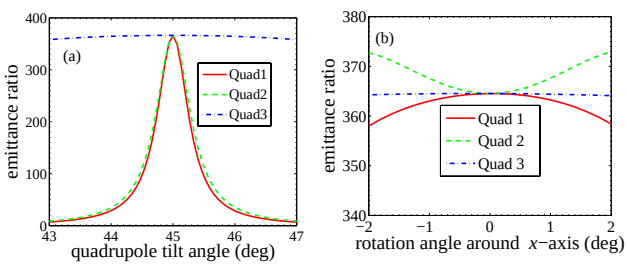

Figure 4: Effects of the quadrupole rotation angles around longitudinal and horizontal axis on the emittance ratio.

In Figure 4 (b), we scan the angle around the horizontal axis (pitch) by $\pm 2^\circ$ using ASTRA . The maximum emittance ratio drop is less than 4%. Similar results are found for the rotation angle around vertical axis (yaw).

Finally we scan quadrupole center locations in each axis by a couple of millimeters. The effect on emittance ratio is comparable to the misalignment in pitch and yaw angles. Usually the quadrupole centers are aligned within 1 mm mechanically.

From simulations shown above, we see that the emittance ratio is neither very sensitive to pitch and yaw rotation, nor to the quadrupole center displacements. Some misalignments, such as center location in z-axis, can be compensated by adjusting the quadrupole strengths. Furthermore, experimentally we do beam-based alignment by using a couple of steering magnets to center the beam on the electromagnetic axes of the quadrupoles. Therefore, the mechanical misalignment of the quadrupole centers, or pitch and yaw angles could be compensated.

However, the emittance ratio is sensitive to errors in the tilt angle of the first two skew quadrupoles. Experimentally, the precision of the alignment of the quadrupole angles is better than $\pm 0.25^\circ$.

CONCLUSIONS

We have investigated analytically the space-charge effects in the rf gun area. An uncorrelated transverse emittance growth is estimated from the non-linear space-charge force, given the initial drive laser spot profiles. The achievable flat-emittance ratio decreases from orders of thousands to hundreds as a result of the un-correlated emittance growth in rf gun. Therefore, the space charge in the gun is the dominant limiting factor for flat-beam production. The most important direction of future R&D is the suppression/compensation of space charge when an axial magnetic field is present on the cathode.

The influences of the skew quadrupole alignments on flat-beam emittance ratio are also studied. Among the six degrees of freedom for each quadrupole, rotations around the longitudinal axis of the first two quadrupoles are found to be the more influential on the flat-beam emittances. It is important to have the high precision control of the quadrupole tilt angles. This might be improved using motorized rotatable mounts for the quadrupoles in order to optimize the rotation online in future experiments.

We would like to thank Court Bohn from Northern Illinois University for valuable discussions.

REFERENCES

[1] A. Burov and V. Danilov, FERMILAB-TM-2043 (1998).

[2] A. Burov, S. Nagaitsev and Ya. Derbenev, Phys. Rev. E **66**, 016503 (2002).

[3] K.-J. Kim, Phys. Rev. ST Accel. Beams **6**, 104002 (2003).

[4] D. Edwards *et al.*, Proceedings PAC2001, pp. 73-75.

[5] K. Flöttmann, "ASTRA: A Space Charge Tracking Algorithm", available at `http://www.desy.de/~mpyflo`.

[6] K.-J. Kim, NIM A275, pp. 201-218 (1989) .